JACS
JOURNAL OF THE AMERICAN CHEMICAL SOCIETY

ARTICLE

pubs.acs.org/JACS

Insights into the Different Dioxygen Activation Pathways of Methane and Toluene Monooxygenase Hydroxylases

Arteum D. Bochevarov,[†] Jianing Li,[†] Woon Ju Song,[‡] Richard A. Friesner,[*,†] and Stephen J. Lippard[*,‡]

[†]Department of Chemistry, Columbia University, New York, New York 10027, United States

[‡]Department of Chemistry, Massachusetts Institute of Technology, Cambridge, Massachusetts 02139, United States

Supporting Information

ABSTRACT: The methane and toluene monooxygenase hydroxylases (MMOH and TMOH, respectively) have almost identical active sites, yet the physical and chemical properties of their oxygenated intermediates, designated P*, H_{peroxo}, Q, and Q* in MMOH and $ToMOH_{peroxo}$ in a subclass of TMOH, ToMOH, are substantially different. We review and compare the structural differences in the vicinity of the active sites of these enzymes and discuss which changes could give rise to the different behavior of H_{peroxo} and Q. In particular, analysis of multiple crystal structures reveals that T213 in MMOH and the analogous T201 in TMOH, located in the immediate vicinity of the active site, have different rotatory configurations. We study the rotational energy profiles of these threonine residues with the use of molecular mechanics (MM) and quantum mechanics/molecular mechanics (QM/MM) computational methods and put forward a hypothesis according to which T213 and T201 play an important role in the formation of different types of peroxodiiron(III) species in MMOH and ToMOH. The hypothesis is indirectly supported by the QM/MM calculations of the peroxodiiron(III) models of ToMOH and the theoretically computed Mössbauer spectra. It also helps explain the formation of two distinct peroxodiiron(III) species in the T201S mutant of ToMOH. Additionally, a role for the ToMOD regulatory protein, which is essential for intermediate formation and protein functioning in the ToMO system, is advanced. We find that the low quadrupole splitting parameter in the Mössbauer spectrum observed for a $ToMOH_{peroxo}$ intermediate can be explained by protonation of the peroxo moiety, possibly stabilized by the T201 residue. Finally, similarities between the oxygen activation mechanisms of the monooxygenases and cytochrome P450 are discussed.

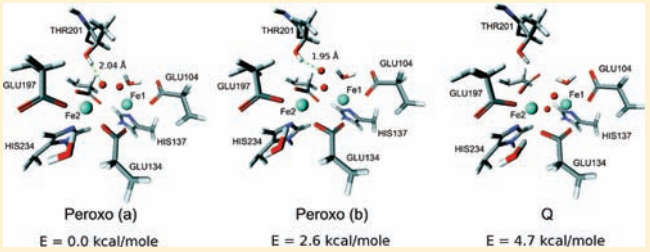

INTRODUCTION

Soluble methane monooxygenase and toluene *o*-xylene monooxygenase belong to the family of bacterial multicomponent monooxygenases (BMMs) that specialize in the transformation of C−H chemical bonds into the C−OH groups for a variety of hydrocarbons.[1−4] Methane monooxygenase hydroxylase (MMOH) has been extensively studied,[5−12] and the toluene monooxygenase hydroxylase (TMOH) has also generated considerable interest[13−16] after its three-dimensional structures became available.[15,17−21] Soluble MMOH enzymes are found in two phylogenetically related proteins, MMOH-Mc and MMOH-Mt, purified from two related organisms, *Methylococcus capsulatus* (Bath) and *Methylococcus trichosporium* OB3b, respectively. A TMOH enzyme similarly occurs in a variety of organisms, two of which will be discussed in this work: toluene/*o*-xylene monooxygenase hydroxylase (ToMOH) and toluene 4-monooxygenase hydroxylase (T4moH), expressed in *Pseudomonas stutzeri* OX1 and *Pseudomonas mendocina* KR1, respectively. These particular variants of MMOH and TMOH have been characterized crystallographically and are most accessible for theoretical analysis. The active sites in each pair are almost identical.

Despite having very similar active sites, the MMOH and TMOH enzymes differ in chemical behavior, something that has puzzled researchers. Not only do they have reactivity specific for distinct types of hydrocarbons, but the properties and the structures of their oxygenated intermediates also differ.[4,13,14] Some light has been shed on the problem after the identification of an extended channel connecting the surface of ToMOH with its active site, a channel that is absent in MMOH.[18] Another advance was the preparation and spectroscopic study of ToMOH mutant forms in which the residue threonine-201, located near the active site, was substituted by other amino acids, serine in particular.[14] Important implications for the kinetics of the reaction and for the catalytic cycle emerged as a result of the substitution.

In the present study we reprise the structural differences between MMOH and TMOH active sites and investigate the energetic consequences of rotation about the threonine $C_\alpha-C_\beta$ bond (T213 in MMOH and T201 in TMOH) by molecular mechanics (MM) and quantum mechanics/molecular mechanics (QM/MM) computational methods. Studying threonine-201 in TMOH and its analog in MMOH is important because understanding their respective abilities to influence the

Received: November 16, 2010
Published: April 25, 2011

dx.doi.org/10.1021/ja110287y | *J. Am. Chem. Soc.* 2011, 133, 7384–7397

chemistry of the diiron sites may be key to the explanation of differences in the intermediates formed by the two proteins. There are several reasons to ascribe a principal role to this threonine residue: (i) It is strictly conserved in the BMM family and located at the active site; (ii) its mutations have a measurable effect on the catalytic mechanism; (iii) its rotational configurations are markedly different in the available crystal structures of MMOH and TMOH forms; (iv) it is involved in an extended hydrogen-bonding network that stretches from the active site to the surface of the protein and may provide a mechanism for proton delivery during the catalytic cycle; and (v) as we demonstrate here, the threonine potential energy profiles correlate strongly with experimentally observed trends in the formation of the hydroxylase intermediates. Based on our theoretical analysis, we formulate a hypothesis that can explain the differences in the behavior of the intermediates and provide further insight into the role that the threonine plays in tuning the chemistry of the BMM enzyme active sites.

The implications of our findings stretch beyond the field of BMM enzymes. The intermediary role of the threonine residue, the proton delivery network fashioned at the diiron site that includes the threonine residue and the neighboring asparagine, and the demonstrated protonation of the peroxo-intermediates in ToMOH reveal strong similarities between the oxidative mechanisms of ToMOH and cytochrome P450.[22,23] We discuss these similarities in more detail in the Relation to Cytochrome P450 Section immediately preceding the conclusion.

It is also important to point out the use of computational methodology in the present paper, as mandated by the objectives of our study. There are many protein pairs in nature that are significantly homologous in structure and similar if not identical in function, as is the case for MMOH and ToMOH. Typically such pairs are analyzed by sequence comparisons, structural superpositions, and other bioinformatics tools, and differences in chemistry are then inferred from data generated in this fashion, leaving much to be understood at an atomic level. Here, we begin with an analysis of this type but proceed to a detailed study of hypotheses emerging from the sequence and X-ray data comparison by using state of the art MM and QM/MM simulations. More generally, the problem we pose from a computational perspective is how to take two extremely complex systems which have a high degree of structural homology and identify precisely what structural elements are responsible for differences in their chemistries. While QM/MM studies focusing on a single protein are common, comparative analyses using high-level computations and successfully making multiple semiquantitative points of contact with experiment are relatively rare. Thus, in addition to being of interest to researchers directly involved in work on MMOH, ToMOH, and related metalloenzymes, such as P450, the description of a successful strategy for using a combination of sequence, structure, high-level energetics, and spectroscopic computations to explicate the differences in related but chemically distinct, protein pairs should be valuable for both theoretical and experimental chemists who wish to understand protein-catalyzed reactions at an atomic level of detail.

COMPUTATION DETAILS

Three computational methods were used in this project to compute energies: MM, QM/MM, and Monte Carlo (MC).

The MM method was applied to generate rotational profiles of serine and threonine in several protein structures. Except when the QM/MM-optimized geometries were available (for the ToMOH protein only), all the crystal structures were obtained from the Protein Data Bank (PDB) and subsequently treated by the independent cluster decomposition algorithm (ICDA) method[24] to assign the positions of the hydrogen atoms and resolve certain misassignments that could be present in the crystal structure. The correct charges of atoms and protonation states of the ligands around the active site were specified manually. As an energy function, the OPLS-AA[25] molecular mechanics force field was used.

The QM/MM method realized in the program QSite[26] and based upon the frozen orbital approach[27−29] for the quantum/classical interface was used to compute high-quality energies of the oxygenated intermediates as well as to minimize their structures. Prior to the QM/MM calculations, the geometry of the MM part of the protein system was optimized with tight convergence criteria. The protonation states of amino acid residues in the protein matrix were assigned based on the distances to neighboring groups which are likely to form a salt bridge. Typically, the cutoff distance for a salt bridge was 3 Å. Multiple residues competing for a salt bridge were resolved manually, with the preference given to the residues located at the shortest distance. The residues on the surface not forming salt bridges were neutralized, and the total charge of all systems studied with QM/MM was kept zero.

The QM part was treated with the B3LYP DFT functional (unrestricted orbitals), while the MM part was handled with the OPLS-AA force field. All QM/MM computations were conducted without cutoffs for electrostatic interactions. For the geometry optimizations, we utilized a smaller basis set (LACVP**[30−32] on iron atoms, and 6-31G* on all other atoms in the QM region) than that with which the single point energy was subsequently computed (LACV3P** on iron atoms, aug-cc-pVTZ without the *f*-functions on the active site waters and the dioxygen, and cc-pVTZ without the *f*-functions on all remaining QM atoms). The antiferromagnetic coupling between the two Fe atoms was treated by the broken symmetry wave function formalism, in the same manner as in our earlier QM/MM study.[10] All the QM/MM energies given in this work correspond to the single point energies obtained with the larger basis set.

In MC sampling of model structures, we used the combination of MC torsion sampling (MCMM) and large-scale low-mode sampling (*l*-LMOD).[33,34] During exploration of the configurational space of the models, the distance between two Fe atoms and the O−O distance in the dioxygen-derived ligand were constrained.

The density functional theory (DFT) optimization of protonated model structures utilized the B3LYP functional, Wachters basis set on Fe atoms, and cc-pVDZ basis set on all the other atoms.

In computing the Mössbauer parameters of the model structures we followed the methodology of isomer shift parametrization and functional/basis set selection from our recent work.[35] The B3LYP functional was used to compute the isomer shift, whereas O3LYP was the functional of choice for the quadrupole splitting parameter. The completely uncontracted Partridge-1 basis set was placed on the iron atoms, and the conventional cc-pVDZ basis resided on the rest of atoms of the model. Our Mössbauer benchmarking study[35] indicates that these are currently the best functional/basis set combinations for the prediction of the isomer shift and the quadrupole splitting parameters. The molecular model systems for Mössbauer calculations were produced from the corresponding active sites by truncation and hydrogen capping.

COMPARISON OF MMOH AND TMOH ACTIVE SITES

To date, almost 30 MMOH and over 10 TMOH crystal structures have been deposited in the PDB. The active sites of all the crystallized MMOH and TMOH forms share a considerable degree of similarity. The identical elements of the immediate coordination environment (the so-called first shell), regardless of

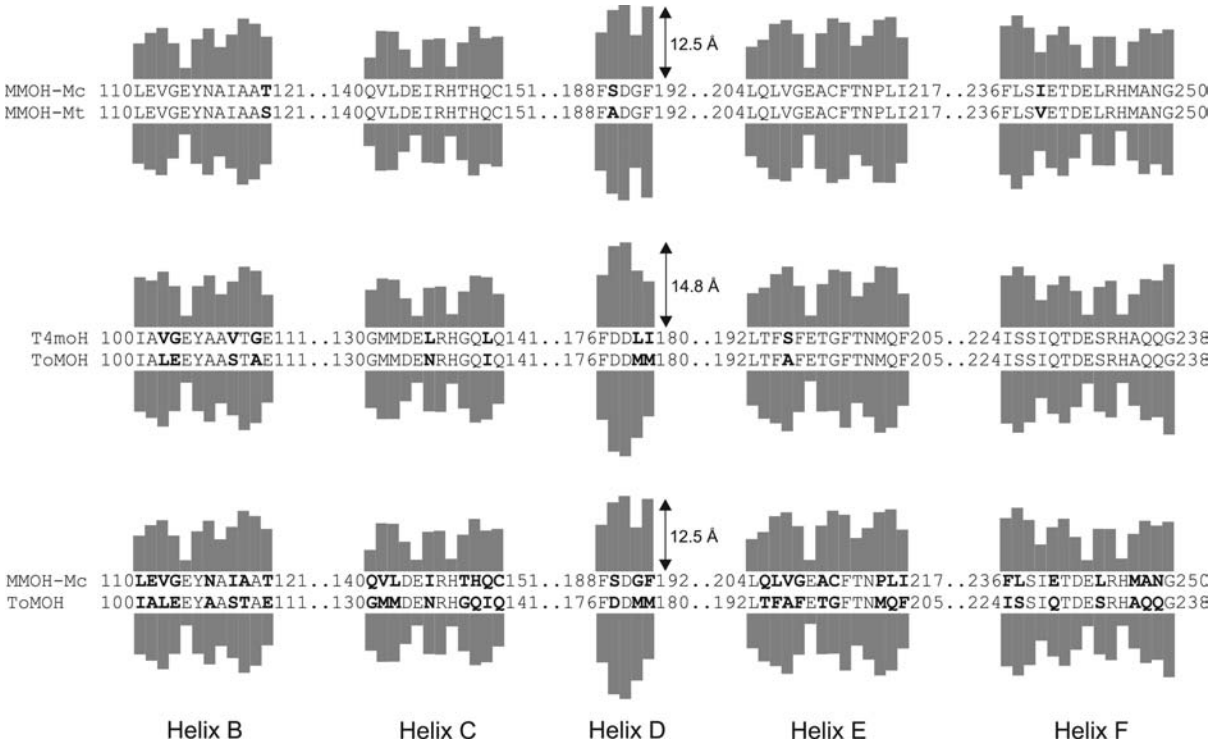

Figure 1. Comparison of the residues around the diiron core in MMOH-Mc (PDB 1MTY), MMOH-Mt (PDB 1MHY), T4moH (PDB 3DHG), and ToMOH (PDB 2INC) crystal structures. The height of the bars above and below the residue codes signifies the approximate distance between the closest atoms belonging to the residue and the diiron core. The substitutions are highlighted in bold.

the oxidation state of the iron atoms, comprise two histidine and four glutamine side chains, with the histidine residues in MMOH and TMOH using different nitrogen atoms to coordinate to the iron atoms.[18] The amino acid residues are fixed elements of the structures, whereas the water molecules, hydroxide ions, and molecules from the crystallization solution that are located in immediate proximity to the iron atoms are variable elements. Their presence fluctuates from structure to structure and depends on the oxidation state of the iron atoms, crystallization conditions, and complex formation with the regulatory protein. The positions of all groups coordinated to iron, including side chains, are subject to translational or rotational modifications. Many amino acids surrounding the coordinating ligands (the second shell) are conserved between MMOH and TMOH, which makes the architecture of their active sites nearly identical.

In any study of the differences in chemistry between MMOH and TMOH intermediates, it is the fixed elements of their active site structures (amino acids) that we have to focus on. As a starting point, it is important to investigate deviations within the MMOH and TMOH structure groups, in order to understand whether we can use one structure as representative of the entire group. MMOH-Mc and MMOH-Mt show almost no variation in the surroundings of the diiron center. Out of the 58 residues located in the active site-forming helices, MMOH-Mc and MMOH-Mt differ only by three (see Figure 1). Only one of these three differences ($V \leftrightarrow I$) is close to the diiron center; however, it involves an inessential residue. A more detailed overall comparison of the two MMOH proteins has been undertaken earlier.[36,37] The mutations differentiating ToMOH from T4moH are more numerous and include 9 out of the analogous 58 residues, but all of them are located relatively far from the diiron center and most of them are inessential for our study (see Figure 1). The number of mutations around the active site agrees with the phylogenetic placement of these proteins[38] based on the entire α-subunit: MMOH-Mc is closer to MMOH-Mt than ToMOH is to T4moH. Notwithstanding these differences, we may conclude that, as far as the chemistry of the active site is concerned, any of the two members of each group may be considered as representative of the group as a whole.

Next, we turn to the differences between the MMOH and TMOH active site environments. Figure 1 reveals a great number of differences: 35 residues out of the 58 do not match when MMOH-Mc and ToMOH sequences are aligned. It is clear that the majority of the changes occur in residues relatively distant from the active site. All residues coordinated to the iron atoms are conserved, but there are several key changes in the 'second' and the 'third' shells. Ones of particular interest, being closest to the active site, are listed in Table 1. Residues not directly coordinated to the diiron center but with side chains that are not obstructed from the diiron center by other residues are considered second shell. This shell may play a direct role by interacting with the variable elements of the active site, such as the dioxygen or water molecules. Residues having some other amino acid chains between them and the diiron center are considered third shell. This shell is considered to be of relatively low importance, although in the catalytic cycle, it could still play a role in stabilizing second-shell conformations.

From Table 1, we can identify important differences in the active sites of MMOH and ToMOH. Substitutions 1, 4, 7, and 8 are not very interesting. The first is not even conserved across both variants of the TMOH family. The side chains of mutations 4 and 7 are relatively distant (about 7 Å) from the diiron center. Substitution 8 deserves somewhat more attention because A235

Table 1. Mutated Residues Closest to the Diiron Center of MMOH-Mc (1MTY) and ToMOH (2INC) [a]

substitution no.	MMOH-Mc	comment	ToMOH	location	conserved?
1	G113	2nd shell	E103	3rd shell, points away from diiron	No[b]
2	T121	3rd shell	E111	2nd shell, H-bond through water with E134	No[c]
3	Q140	2nd shell, H-bond with E144	G130	3rd shell	Yes
4	T148	2nd shell, points away from diiron	G138	3rd shell	Yes
5	Q205	3rd shell	T193	2nd shell	Yes
6	I217	2nd shell	F205	2nd shell	Yes
7	E240	3rd shell, points away from diiron	Q228	3rd shell, points away from diiron	Yes
8	M247	3rd shell, points away from diiron	A235	2nd shell	Yes

[a] The column 'conserved?' indicates whether the shown mutation is shared by all the members of the groups MMOH and TMOH. [b] E103 in ToMOH and G103 in T4moH. [c] T121 in MMOH-Mc and S121 in MMOH-Mt.

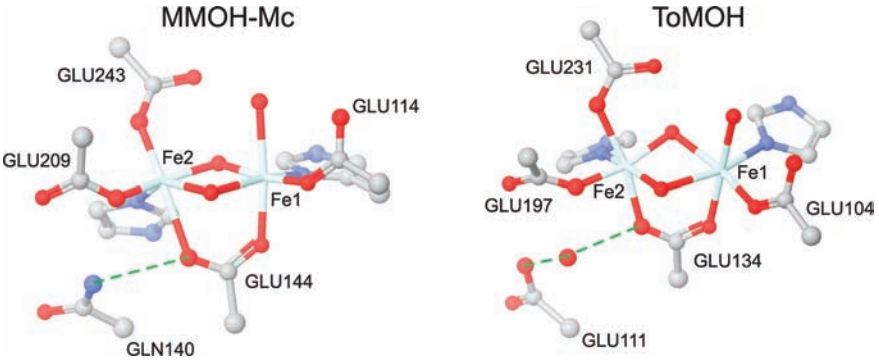

Figure 2. The hydrogen bonds (traced with the dashed green lines) formed by the bridging carboxylate and preserved in MMOH-Mc and ToMOH crystal structures despite the mutations in the second shell residues. The color-coding is as follows: carbons are gray, oxygens are red, nitrogens are blue, and irons are cyan. Hydrogen atoms are omitted for clarity.

of the ToMOH family is located in the second shell. However, its importance is not clear. The other four mutations are more significant. Substitution 2 is not conserved in both variants of the MMOH family, but the residues associated with this substitution in MMOH-Mc and MMOH-Mt have a functionally similar side chain: threonine and serine, respectively, so that we may consider it to be effectively conserved. Alteration T121 (MMOH) → E111 (ToMOH) is unusual. The side chain of E111 is apparently hydrogen bonded to a water molecule, which is in turn hydrogen bonded to the critical residue E134 serving as a ligand for the diiron center (see Figure 2). T121 of MMOH does not form hydrogen bonds with E144, and therefore substitution T121 (MMOH) must play a role different from → E111 (ToMOH). Interestingly, substitution T121 (MMOH) → E111 (ToMOH) is complementary to substitution number 3 in Table 1: Q140 (MMOH) → G130 (ToMOH). The backbone of Q140 (MMOH) is aligned with the backbone of G130 (ToMOH). But G130 (ToMOH) has only a hydrogen atom for a side chain and cannot carry out the apparently important function similar to that of Q140 in MMOH. This function in ToMOH is accomplished by the side chain of E111, even though its backbone is not aligned with that of MMOH Q140. Backbones of MMOH Q140 and ToMOH E111 are not aligned, but their side chains have the same function in the stabilization of the active site. The role and the significance of this hydrogen bond are currently not understood. Substitution 6 changes the aliphatic hydrophobic group of isoleucine into the aromatic hydrophobic group of phenylalanine in the second shell of both protein subfamilies. Whether the presence of the phenyl ring in the second shell of ToMOH might lead to a $\pi-\pi$ interaction with the aromatic substrate is unknown but should not be discounted. The analogous residue in aromatic-oxidizing phenol monooxygenase is also phenylalanine.[39]

It is unlikely that any single substitution of those just discussed will explain the profoundly dissimilar scenarios by which dioxygen is activated in MMOH and TMOH. It is more probable that the effect of these substitutions is cumulative and that they all contribute to the observed differences. Moreover, studying the changes provides just one window on understanding differences in the MMOH and TMOH catalytic cycles. At least two additional resources remain. The first is the effect of the regulatory protein on the secondary structure of helix E and the presence of an additional ordered water molecule in the vicinity of the diiron core. The ability to observe catalytic intermediates in the MMOH and ToMOH reaction cycles requires the presence of the respective regulatory proteins. The second resource is the rotatory conformation of the conserved threonine T213 in MMOH and T201 in TMOH, vide infra.

We now briefly discuss the effects of the regulatory protein binding on structure before moving to the rotameric forms of of the threonine, which comprise the key subject of this work. Out of the four proteins that we compared, only one was crystallized in complex with its regulatory protein, T4moH,[21] hereafter referred to as T4moHD. There are two noticeable modifications from the structure of the hydroxylase in the absence of the regulatory protein. The first is a distortion of helix E, which affects the secondary structure of two residues, T201 and N202, involved in a hydrogen-bond network leading from the surface of

dx.doi.org/10.1021/ja110287y |J. Am. Chem. Soc. 2011, 133, 7384–7397

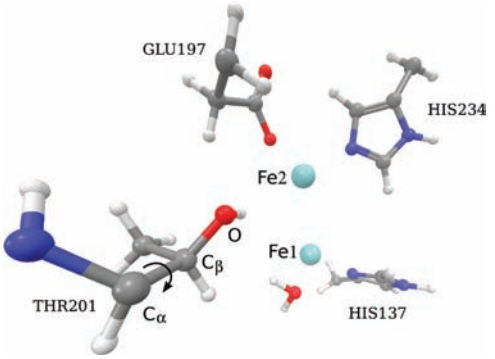

Figure 3. The locations of the two iron atoms and C_β and O atoms of threonine (or serine in the mutant) relative to one another. These atoms form the Fe1−Fe2−C_β−O dihedral angle denoted 2Fe-THR in the text. The arrow shows a rotation around the C_α−C_β bond used to construct plots in Figures 6 and 7.

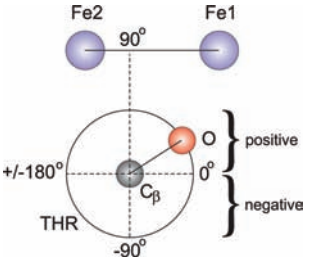

Figure 4. A schematic projection down the C_α−C_β bond of the threonine (or serine) C_β−O bond onto the plane in which two iron atoms lie and which is perpendicular to the C_α−C_β bond. This projection reveals that when dihedral angle Fe1−Fe2−C_β−O changes (due to rotation around C_α−C_β bond of threonine), the distance between the hydroxyl oxygen and the diiron center also changes. The positions and the values of four Fe1−Fe2−C_β−O angles (0°, ±90°, ±180°) in the projected picture are shown. Because threonine is allowed to move parallel to the line connecting the iron atoms, a particular dihedral angle does not necessarily indicate the proximity of the oxygen atom to the diiron center. For this reason, the distances Fe_1−O and Fe2−O are used in addition to the Fe1−Fe2−C_β−O angle in Table 2 to indicate the nearness of the threonine hydroxyl group to the diiron center.

the protein to the active site and is thought to be important for the proton shuttling.[39] As a result of this distortion, T201 and N202 no longer reside in the α-region of the E helix but belong to a transitional structure between α and π helices. As a further consequence, T201 recedes from the diiron center; the distance from its backbone oxygen atom to Fe_2 increasing from 5.36 Å to 6.26 Å. The regulatory protein thereby creates some extra space between the diiron core and the residues T201, Q228, and F205 located just beside it. The other modification is the presence of a new water molecule apparently hydrogen bonded to the water molecule coordinated with Fe1. It is located in the extra space just mentioned. The presence of this additional water molecule may have important implications for the hydrogen-bond network extending to the surface of the protein and for the role it may play in the formation of a peroxo species; the latter point is discussed below. These changes brought about by the regulatory protein in T4moH are noteworthy, but whether they are mirrored in ToMOH and, most importantly, the MMOH proteins is currently unknown. When a crystal structure for the corresponding MMOH and its cognate regulatory protein MMOB becomes available for one of the MMOH proteins, it will be clear whether the regulatory protein has an identical structural role, or, perhaps, induces a distinct set of changes that might contribute to factors that distinguish the chemical properties of the MMOH and TMOH intermediates.

■ THREONINE CONFORMATIONS IN MMOH AND TOMOH CRYSTALS

In this section we describe the rotatory conformations of the threonine residues observed in MMOH and TMOH crystal structures and discuss the consequences that these conformations might have for stabilizing the catalytic intermediates. The next section will focus on the rotational energy profiles.

In order to quantify the rotational configurations we refer to the dihedral angle Fe1−Fe2−C_β−O illustrated in Figures 3 and 4, hereafter 2Fe-THR. Positive values of the dihedral angle represent the situation when the threonine hydroxyl group turns toward the diiron center and when negative values correspond to the opposite orientation. Because the C_α backbone carbon atom to which the threonine hydroxymethyl group is attached may shift slightly from structure to structure, the value of the dihedral angle does not necessarily define the distance of the oxygen atom to the diiron center, which would correlate with the possibility of threonine participation in dioxygen activation. We therefore require additional geometrical information to describe this structural element. Tables 2 and 3 contain this additional information and include the rotatory geometry of threonine with respect to the diiron center. These tables clearly reveal that positive 2Fe-THR dihedral angles signal a significantly shorter (about 1 Å) distance from the threonine hydroxyl group to the diiron core. An interesting caveat is the set of distances for T4moHD. For this structure, a positive dihedral angle corresponds to d_{Fe1}−O and d_{Fe2}−O distances that are about the same as those in other proteins where the dihedral angle is negative. This result occurs because the regulatory protein distorts the secondary structure of helix E and drives T201 away from the diiron site by about 1 Å. Presumably, the structures of MMOH and/or ToMOH in complex with their respective regulatory proteins would have similarly negative dihedral angles, with distances that are larger than those corresponding to the positive angle.

Another observation that follows from the tables is the striking difference in dihedral angles for the MMOH and TMOH structures. If we disregard soaked structures, which are likely to have distorted and unnatural geometries, then we can conclude that in MMOH the threonine hydroxyl is rotated in a direction away from the diiron center, whereas in ToMOH it always faces the iron atoms. As discussed below, we believe that the difference has far-reaching implications for the stability of the peroxo intermediates with respect to conversion to the hydroxylating intermediate Q in MMOH. The distance between the threonine hydroxyl oxygen atom and the diiron core, even in the case of a positive dihedral angle, is too large to allow a direct interaction between the two. But when we consider that a peroxo ion O_2^{2-} can be positioned between the threonine and the iron atoms, the distance appears just right. Our QM/MM optimizations on ToMOH predict that a strong hydrogen bond will form between the threonine OH group and the coordinated peroxo ion. Such an interaction helps make the peroxo structure 4.7 kcal/mol more stable than a Q-type intermediate, a putative di(μ-oxo)diiron(IV) unit in which the O atoms are too far away from the threonine to form a hydrogen bond.

Table 2. Rotational Conformations of T213 in MMOH with Respect to the Diiron Center in a Variety of Crystal Structures[a]

structure	protein	oxidation state	2Fe-THR, deg	d_{Fe1}−O, Å	d_{Fe2}−O, Å	χ, deg	comment
1XU3	MMOH-Mc	+3, +3	109.0	6.02	5.61	113.8	soaked in bromophenol
			163.1	6.66	5.42	75.2	
1XU5	MMOH-Mc	+3, +3	−89.4	7.13	6.65	−48.2	soaked in phenol
			164.7	6.56	5.54	72.3	
1XVB	MMOH-Mc	+3, +3	−153.8	7.82	6.55	−68.9	soaked in 6-bromohexanol
			−155.6	7.86	6.53	−67.1	
1XVC	MMOH-Mc	+3, +3	−78.0	7.08	6.63	−58.8	soaked in 8-bromooctanol
			−77.5	6.91	6.37	−61.0	
1XVD	MMOH-Mc	+3, +3	−76.8	6.76	6.45	−59.4	soaked in 4-fluorophenol
			160.6	6.53	5.45	77.5	
1XVE	MMOH-Mc	+3, +3	−77.9	7.29	7.10	−61.1	soaked in 3-bromo-3-butenol
			−100.9	7.71	7.23	−42.3	
1XVF	MMOH-Mc	+3, +3	−81.1	7.16	6.80	−56.6	soaked in chloropropanol
			−109.8	7.38	6.81	−26.3	
1XVG	MMOH-Mc	+3, +3	155.6	6.36	5.22	78.8	soaked in bromoethanol
			168.8	6.55	5.63	69.4	
1XMF	MMOH-Mc	+3, +3	−75.3	6.80	7.09	−70.7	Mn replaces Fe; soaked
			−89.6	7.09	7.07	−60.0	
1XMH	MMOH-Mc	+2, +2	−87.0	7.28	6.95	−59.4	Co replaces Fe
			−92.4	7.27	6.82	−50.9	
1FZ0	MMOH-Mc	+2, +2	−74.7	7.32	6.76	−46.7	
			−80.7	7.37	6.62	−53.9	
1FZ1	MMOH-Mc	+3, +3	−89.2	7.19	6.80	−48.4	
			162.1	6.65	5.60	73.5	
1FZ2	MMOH-Mc	+2, +3	−69.8	7.21	6.61	−56.2	soaked
			−71.7	7.28	6.64	−54.3	
1FZ3	MMOH-Mc	+3, +3	169.0	6.62	5.66	68.3	soaked at pH 6.2 (0.1 M PIPES)
			−84.9	6.96	6.29	−55.9	
1FZ4	MMOH-Mc	+3, +3	−82.7	6.94	6.45	−53.4	soaked at pH 8.5 (0.1 M TRIS)
			−82.7	7.10	6.42	−54.6	
1FZ6	MMOH-Mc	+3, +3	−77.8	7.09	6.81	−16.7	soaked in 1 M methanol
			−112.9	7.22	6.60	−59.0	
1FZ7	MMOH-Mc	+3, +3	−68.8	6.69	6.53	−70.3	soaked in 0.9 M ethanol
			161.9	6.56	5.58	70.6	
1FZ8	MMOH-Mc	+3, +3	21.7	6.00	6.13	−171.1	soaked in bromoethane
			176.6	6.72	5.72	65.5	
1FZ9	MMOH-Mc	+3, +3	−85.2	7.31	6.61	−53.1	soaked in iodoethane
			100.1	6.59	7.20	−54.2	
1FZH	MMOH-Mc	+3, +3	−70.6	6.58	6.24	−66.4	pressurized with xenon
			−178.9	6.36	5.50	54.8	
1FZI	MMOH-Mc	+3, +3	−68.1	6.85	6.97	−62.0	pressurized with xenon
			−58.9	7.00	6.91	−75.7	
1MHY	MMOH-Mt	+3, +3	−87.6	6.77	6.23	−46.0	
1MHZ	MMOH-Mt	+3, +3	−97.5	6.75	6.03	−43.6	
1MTY	MMOH-Mc	+3, +3	−72.5	7.10	6.80	−61.9	
			−58.2	6.91	6.80	−75.7	
1MMO	MMOH-Mc	+3, +3	−90.1	6.99	6.41	−48.5	
			−90.5	7.03	6.45	−48.0	

[a] The distances d_{Fe1}−O and d_{Fe2}−O are measured between the corresponding iron atom and the oxygen of the threonine hydroxyl group; the dihedral angle 2Fe-THR (Fe1−Fe2−C_β−O) is illustrated by Figures 3 and 4. The dihedral angle N−C−C_α−O characterizing the internal rotation of the threonine is also given and denoted χ. The two values given for each entry correspond to the two different protomers of MMOH-Mc. The crystal structure notation corresponds to that of the PDB.

Figure 5 shows the active site geometries of the two lowest-energy peroxo intermediates and a Q-type intermediate predicted by the QM/MM optimization starting from the ToMOH 2INC crystal structure. The relative energies of these

dx.doi.org/10.1021/ja110287y |J. Am. Chem. Soc. 2011, 133, 7384–7397

Table 3. Rotational Conformations T201 in TMOH with Respect to the Diiron Center in a Variety of Crystal Structures[a]

structure	protein	oxidation state	2Fe-THR, deg	$d_{Fe1}-O$, Å	$d_{Fe2}-O$, Å	χ, deg	comment
3I5J	T4moHD	+3, +3	141.2	7.37	6.24	58.9	
3I63	T4moHD	+3, +3	139.4	7.32	6.19	56.2	H_2O_2 is loosely bound to Fe atoms
3DHG	T4moH	+3, +3	156.0	6.45	5.36	66.5	
			135.3	6.48	5.27	78.5	
3DHH	T4moHD	+3, +3	136.6	7.37	6.26	57.9	
3DHI	T4moHD	+2, +2	137.6	7.33	6.64	58.9	
2RDB	ToMOH	+3, +3	157.4	7.03	5.67	64.6	I100W mutant
2IND	ToMOH	+2, +2	164.9	7.13	5.98	64.9	Mn replaces Fe
2INC	ToMOH	+3, +3	161.8	6.71	5.62	64.0	
1T0Q	ToMOH	+3, +3	164.4	6.88	5.74	66.0	
1T0R	ToMOH	+3, +3	147.8	6.67	5.45	78.5	with azide bound
1T0S	ToMOH	+3, +3	179.7	6.84	5.65	57.6	soaked in 4-bromophenol

[a] The distances $d_{Fe1}-O$ and $d_{Fe2}-O$ are measured between the corresponding iron atom and the oxygen of the threonine's hydroxyl group; the dihedral angle 2Fe-THR (Fe1−Fe2−C_β−O) is illustrated in Figures 3 and 4. The dihedral angle N−C−C_α−O characterizing the internal rotation of the threonine is also given and denoted χ. The crystal structure notation corresponds to that of the PDB.

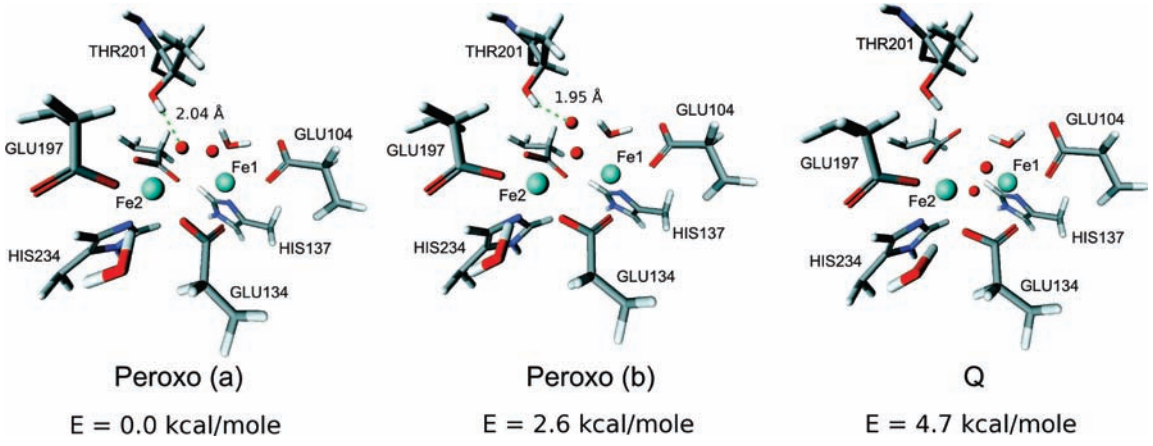

Figure 5. The two lowest-energy ToMOH peroxo structures (left, *cis*-μ-1,2, and center, μ-1,1) and the Q structure (η^2,η^2) optimized with the QM/MM method (B3LYP/OPLS2001); the only unlabeled residue is GLU231. Their relative energies computed in the larger basis set are given below. The dashed green lines indicate the hydrogen bonds formed between the T201 residue and the peroxide ion. The color-coding is as follows: hydrogens are white, carbons are gray, oxygens are red, nitrogens are blue, and irons are cyan.

structures are also shown. One other peroxo intermediate found in the course of optimization did not form a hydrogen bond with T201 and was several kcal/mol higher in energy than the Q structure. We therefore ascribe to this hydrogen bond the stabilization effect that helps make the peroxo more favorable than Q. In contrast, our previous QM/MM study of MMOH predicted almost identical energies for the peroxo and Q structures.[10] The peroxo structure in that study had no possibility to form a hydrogen bond with T213, which was pointed away from the active site and therefore could not be stabilized by such an interaction. The present findings agree well with experimental observations. In MMOH, the peroxo intermediate transforms spontaneously into Q, which serves as the principal substrate oxidizing agent.[6] In ToMOH, intermediate Q is not observed, and oxidation is performed by a peroxo species.[13] Our conclusion is further supported by the fact that the peroxo intermediates of MMOH and ToMOH have very different quadrupole splittings in their Mössbauer spectra, 1.51 mm/s in both MMOH-Mc and MMOH-Mt and 0.67 mm/s in ToMOH. Such different quadrupole splittings indicate a different geometry of the active site or a different protonation state. The observation that the threonine may stabilize the peroxo intermediate in TMOH but not in MMOH is thus in accord with the thermodynamics and compatible with the Mössbauer measurements.

During the course of our QM/MM studies of the ToMOH protein using the 2INC crystal structure as the starting geometry, the crystal structure of T4moH in complex with its regulatory protein (PDB 3DHH) became available. The latter structure is valuable for theoretical modeling of the TMOH catalytic cycle because the regulatory protein is essential for the efficiency of the oxidation and because it is also complexed to either T4moH or ToMOH in most experiments. As we have already mentioned, and as evident from the data in Table 3, the regulatory protein increases the distance between the threonine side chain and the diiron center by about 1 Å. This change makes it much more difficult for a strong hydrogen bond OH···O−O, such as that observed in the peroxo structures based on the 2INC geometry, to occur. However, formation of the complex between T4moH and its regulatory protein brings an additional water molecule to the active site cavity that is situated between the diiron center and

dx.doi.org/10.1021/ja110287y |*J. Am. Chem. Soc.* 2011, 133, 7384–7397

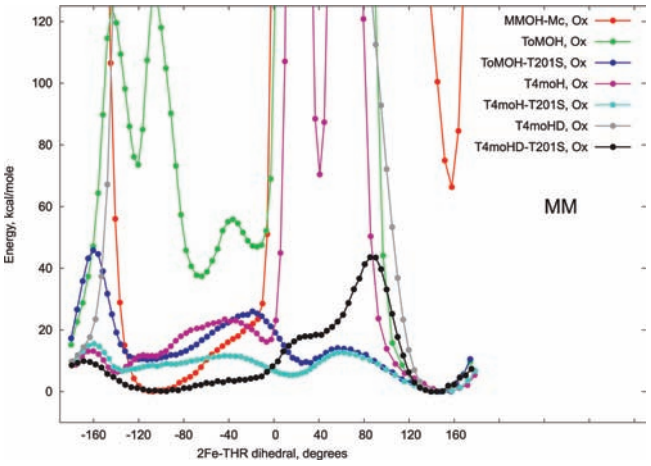

Figure 6. Rotation profiles of threonine in various MMOH and TMOH proteins computed with the MM method. In MMOH, threonine corresponds to T213, and in TMOH, it stands for T201. The T201S mutant curves were produced by replacing the methyl group in the corresponding threonine crystal structures with a hydrogen atom.

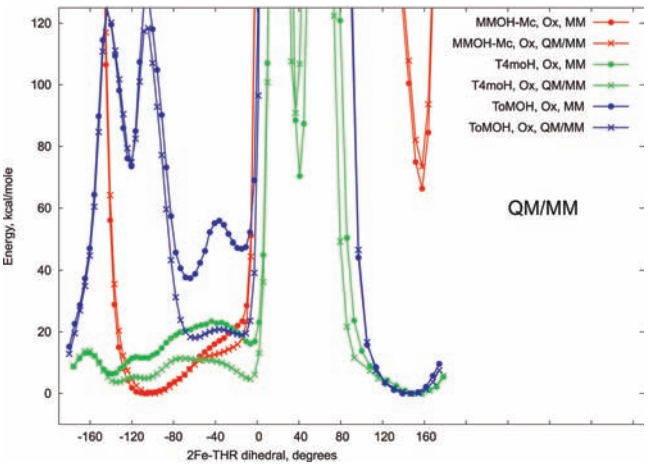

Figure 7. Rotational profiles of threonine in various MMOH and TMOH proteins computed with the QM/MM method. In MMOH, threonine corresponds to T213, and in TMOH it stands for T201.

the threonine hydroxyl. It is conceivable, therefore, that stabilization of the peroxo intermediate in the presence of the regulatory protein occurs through this water filling in the extra 1 Å of space between the threonine OH group and the peroxo ion. Currently we are investigating this hypothesis by studying the intermediates by the QM/MM method starting from the T4moHD crystal structure. In addition, the peroxo ion may be protonated,[14,17,40] which permits other patterns for the hydrogen-bond network between the peroxo ion and the threonine hydroxyl group, as is discussed next Section.

THREONINE ROTATIONAL ENERGY PROFILES

The mutation of ToMOH T201 into a very similar residue, serine, leads to significant changes in the oxidation chemistry of the reduced hydroxylase.[14] Judging from the Mössbauer and optical spectra, when in complex with the regulatory protein (ToMOD), the mutant produces two types of peroxo structures upon reaction with O_2: the $ToMOH_{peroxo}$ and $T201_{peroxo}$ species. The ratio of the concentrations of the two types of the diiron intermediates is approximately 1:1.[17]

The hypothesis set forth in the previous section proposes that an MMOH-like peroxo, $T201_{peroxo}$, can be formed when the threonine points its hydroxyl group away from the diiron center. According to this hypothesis, the Thr→Ser mutation must facilitate the rotation around the $C_\alpha-C_\beta$ bond. As an evaluation of this suggestion and possibly to provide a verification of our hypothesis, we carried out a straightforward computational study in which a series of single-point energies were generated for different dihedral angles 2Fe-THR and in which all other atoms not participating in the rotation were frozen. We also considered whether the regulatory protein would have any effect on the barrier to rotation, because in T4moHD it notably affects the position of the threonine compared to wild-type T4moH.

Threonine rotation was studied by two computational methods: MM and QM/MM. The first is more suitable for faster but less accurate work, whereas the second is good for more accurate, quantitative analysis albeit computationally much more expensive. We applied the MM method to probe the problem and to formulate initial conclusions and then repeated the most interesting rotational profiles by using the QM/MM method, to ascertain the quality of the MM results.

Figure 6 superimposes threonine or serine rotational profiles for the oxidized states of six different proteins: MMOH-Mc, ToMOH, ToMOH-T201S, T4moH, T4moH-T201S, and T4moHD-T201S. The energy is plotted as a function of the dihedral angle 2Fe-THR rather than the χ (N−C−C−O) angle around which the rotation was actually performed. The functional transformation of χ into Fe1−Fe2−C_β−O is important because the value of χ does not necessarily relate to the distance of the threonine hydroxyl with respect to the diiron center, and this position is key in our discussion. Moreover, the backbone deformation effected by the regulatory protein in T4moHD makes the same values of the χ angle (in, say T4moH vs T4moHD) correspond to substantially different positions of the hydroxyl with respect to the diiron core, so that comparing χ angles in different proteins for the sake of evaluating our idea about the threonine rotation becomes problematic. Note, for example, the different regions to which the experimental χ angles belong in the nondeformed TMOH and TMOHD crystal structures.

As indicated in the diagram of Figure 4, positive values of the 2Fe-THR angle in Figure 6 reflect the situation when the OH group is directed toward the iron atoms, whereas negative angles are for the OH group pointing *away* from the iron atoms. In MMOH and ToMOH the rotation energy minima are located approximately at −102.9 and 139.2 corresponding to χ angles of −40 and 85.0. The change of the minima compared to the 2Fe-THR angles observed in the corresponding crystal structures is most likely due to the crystal structure relaxation during the theoretical modeling plus the inherent limited accuracy of the MM method, although the latter is expected to have a small contribution to the error. The change in shift is less pronounced in terms of the χ angle, which suggests that the relaxation affects the diiron core more than it does the side chain of the threonine.

Figure 6 clearly demonstrates several important points about the structural properties of the threonine in the MMOH and TMOH proteins. First, it confirms the pattern observed earlier for the crystal structures of the wild-type MMOH and TMOH. The hydroxyl group in MMOH strongly prefers negative angles, whereas in TMOH it assumes a different configuration, with

dx.doi.org/10.1021/ja110287y |*J. Am. Chem. Soc.* 2011, 133, 7384–7397

positive angles. Even though ToMOH (green curve) has high-energy rotational minima corresponding to the negative angle, the very high barriers separating negative angles from positive angle minima do not leave the $C_\alpha-C_\beta$ bond much kinetic possibility to rotate. The rotation in the T4moH (magenta curve) is much less restricted. One of the barriers gets significantly smaller, and the energy of the MMOH-type threonine rotational configuration is higher than the absolute minimum by over 6 kcal/mol (compare with roughly 38 kcal/mol in the case of ToMOH). Nevertheless, the TMOH-type configuration should be highly predominant, even in T4moH.

Second, the association of the regulatory protein with T4moH changes the rotational energy landscape dramatically (compare the magenta and gray curves). The regulatory protein totally prohibits rotation of the hydroxyl by imposing an enormously high barrier, which essentially freezes the rotation to adopt the configuration where the OH group faces the active site. Possibly, in this manner it imposes a certain specificity for the formation of only one type of peroxo intermediate, compared with the case of the ToMOHD-T201S mutant discussed below. Because the crystal structure of ToMOHD is unavailable, we were not able to check what effect the regulatory protein has on ToMOH or its mutants, but we expect it to be very similar to the effect observed in T4moHD.

Third, the mutation of the threonine into serine in the TMOH proteins produces another dramatic change in the rotational energy curves. While preserving the absolute minima at the positive angles, the energies of the local minima at the negative angles are drastically reduced. Additionally, the barriers to rotation fall sharply in magnitude so that rotation around the $C_\alpha-C_\beta$ bond and the population of both configurations (MMOH-like and TMOH-like) become possible. The effect is most pronounced when the regulatory protein associates with T4moH (black curve). The MMOH configuration in this case is separated from TMOH by only 9.9 kcal/mol of a barrier and lies higher only by 0.2 kcal/mol. This energy profile qualitatively agrees with the experimental observation that the ToMOHD-T201S mutant generates two peroxo forms in comparable proportion. The energy difference of 0.2 kcal/mol closely corresponds to the ratio of 1:1 that would be predicted using the $\exp(-\Delta H/kT)$ formula, if we assume that $\Delta E \approx \Delta H$ and use the temperature of 277 K at which the experiment was performed. However, beside the $\Delta E \approx \Delta H$ approximation, we have to remember that the two forms with comparable concentrations were observed on ToMOHD-T201S, and not T4moHD-T201S, the energy profile of which we are currently discussing. Additionally, we do not currently know the structure of peroxo TMOH, and so it would be difficult to model its threonine rotation profile. Our preliminary calculations based on the ToMOH (a) peroxo model from Figure 5 indicate that the presence of O_2^{2-} in the active site, and even the formation of the hydrogen bond between O_2^{2-} and T201 does not significantly alter the general shape of the ToMOH (Ox) curve. These several approximations allow us to conclude that the energy separation of 0.2 kcal/mol obtained from the T4moHD-T201S curve and the ratio of the comparable peroxo populations in the experiment are in an excellent qualitative agreement. Overall, the rotational energy profiles in Figure 6 reveal the major influence of the regulatory protein and also explain how the threonine mutation into serine can lead to a formation of both peroxo structure types.

Figure 7 compares several MM rotational energy curves with QM/MM curves for the same structures. The QM/MM method, based on the B3LYP DFT functional, should be considered significantly more accurate than MM. We must remember, however, that B3LYP itself is not without defects, especially when metal atoms are present, and so its predictions should be viewed with caution. Because the QM/MM method is much more computationally expensive than MM, it would be wasteful to apply QM/MM if the accuracy of MM is sufficient. Therefore, the goal of the comparison in Figure 7 is to ascertain whether the MM energy profiles can be trusted without the recourse to the QM/MM method. From Figure 7 we note that MM and QM/MM agree almost quantitatively in the regions of the 2Fe-THR from −180 to −140 and from 100 to 180 of the 2Fe-THR angle. The agreement in the region from −140 to −100 is only qualitative, with the differences in energy bewteen QM/MM and QM in some cases over 30 kcal/mol, but the shapes of the corresponding QM/MM and MM curves are similar throughout. This region of qualitative agreement contains the MMOH-like minima and is thus a potentially important span of angles. These or other QM/MM curves that we computed (not shown) did not alter our qualitative conclusions regarding the role of the regulatory protein and the effect of the mutation, but should more quantitative calculations be made in the future (especially with the goal of computing ΔG, and not only ΔE), the QM/MM method should be chosen.

A recent experimental study[17] describing crystal structures and dioxygen activation characteristics of several ToMOH mutants (T201S, T201G, T201C, and T201V) confirms our rotational profiling. T201S is crystallized with the hydroxyl group of serine-201 pointing toward the diiron center with the corresponding 2Fe-THR angle equal to 141°, in agreement with the ToMOH-T201S curve in Figure 6. It is interesting that T201G displays a small amount of catalytic activity, even though it cannot form a hydrogen bond with the peroxo group. A plausible explanation for this result is that glycine, being small and nonhydrophobic, lets an extra water take the place of an otherwise bulky residue. This water might assist in stabilizing the corresponding peroxo species and in proton delivery during the catalytic cycle. The T201 V mutant, having a bulky and hydrophobic residue is, not surprisingly, the least active.

■ MÖSSBAUER SPECTRA AND PROPOSED STRUCTURES OF THE PEROXO INTERMEDIATES

The remaining issue of interest is the nature of the geometrical structures of the peroxo intermediates for MMOH and TMOH proteins. In the previous section we showed that the appearance of one or another peroxo intermediate, or both, as in the case of the T201S mutant, in the experiment correlates well with the position of the energetic minima on the threonine rotation energy profile. In an earlier section, we showed that the QM/MM optimization predicted two $ToMOH_{peroxo}$ structures stabilized by a hydrogen bond formed between T201 and the peroxo ion, a geometry that would be impossible for MMOH. There has been disagreement in the past over the structure of the peroxo intermediate in MMOH, in particular, whether it has the η^2,η^2 or *cis*-μ-1,2 geometry.[10,41−43] In any case, neither of these geometries can form a hydrogen bond with T213 because the distance is too long, and therefore the structure may differ from the types illustrated in Figure 5.

The geometrical differences between the ToMOH structures and their lower energy with respect to a Q-type structure are consistent with the experimental failure to detect the latter in this enzyme. However, the peroxo structures shown in Figure 5 cannot be *exactly* correct for at least two reasons. First, they were

Table 4. Computed Mössbauer Characteristics of Some Geometrical Models of the ToMOH Intermediates Whose Structures Are Shown in Figure 5

form	Fe	oxidation state	spin	δ_{exp}, mm/s	$\lvert\Delta E\rvert_{exp}$, mm/s	δ, mm/s	$\lvert\Delta E\rvert$, mm/s
peroxo (a)	Fe1	+3	+5	0.54	0.67	1.02	3.02
	Fe2	+3	−5	0.54	0.67	0.65	0.44
peroxo (b)	Fe1	+3	+5	0.54	0.67	1.00	2.71
	Fe2	+3	−5	0.54	0.67	0.59	0.34

optimized starting from a ToMOH structure not associated with ToMOD. The crystal structure of T4moHD, an excellent model for ToMOHD, revealed that there is additional space occupied by an extra water molecule separating T201 and the diiron center, by comparison with T4moH, so that the hydrogen-bond formation *directly* between T201 and the peroxo ion coordinated to the iron atoms would be unlikely. Second, the Mössbauer characteristics that we computed for these structures deviate widely from the experimentally observed values (see Table 4). At the same time, the theoretically predicted Mössbauer spectra of MMOH peroxo candidates agree well with the experiment.[41,35] Nevertheless, we still present and discuss these peroxo structures because for the first time they illustrate the kinds of structural elements that might explain the different chemical behavior of the MMOH and TMOH intermediates and serve as a first approximation for forthcoming modeling. Importantly, through certain modifications in the geometries it is possible to eliminate both obstacles mentioned above and reconcile theory with experiment. The rest of this section explains how.

As the rotational energy profiles of T201 suggest and as proposed in the literature[14,40] based on experimental studies, T201 must participate in the stabilization of the TMOH peroxo intermediate. The water molecule that accompanies binding of the regulatory protein can serve as a hydrogen-bonding bridge between the peroxo ion and the threonine side chain. Possible hydrogen-bond networks between O_2^{2-} and T201 through the water molecule are shown in Figure 8. Such networks may involve protonation, as, for example, models (a) and (b), and this proton can be carried by the extra water molecule as H_3O^+. In Figure 8 we placed the proton on the peroxide anion, the most basic species. However, when the oxygen-containing species is bound to the two Fe(III) ions, its basicity will change. Other modes of coordination of O_2^{2-} with the diiron center are possible, and the choice of the μ-1,1 coordination in Figure 8 is purely for illustrative purposes. Both the μ-1,1 and μ-1,2 binding modes, for example, provide just enough space for the protonated peroxo ion and the water molecule hydrogen bound to it to fit between the diiron center and the threonine residue. A detailed study of the relative stabilities of such structures will be the subject of a separate study. Here we are only concerned with proposing how peroxo structures, such as those in Figure 5, could be modified in the presence of the regulatory protein so that T201 can be involved in the stabilization of the peroxo structure despite the increased distance between the O_2^{2-} and the hydroxyl group.

The next task is to explain why the Mössbauer spectra of the MMOH- and TMOH-type peroxo species are different from one another. The MMOH peroxo intermediate displays only one signal with an isomer shift δ and a quadrupole splitting ΔE_Q equal to 0.66 and 1.51 mm/s, respectively.[6] The Mössbauer parameters of the TMOH-type peroxo are: δ = 0.55 and ΔE = 0.67 mm/s, also comprising only one signal.[13] Although there is a

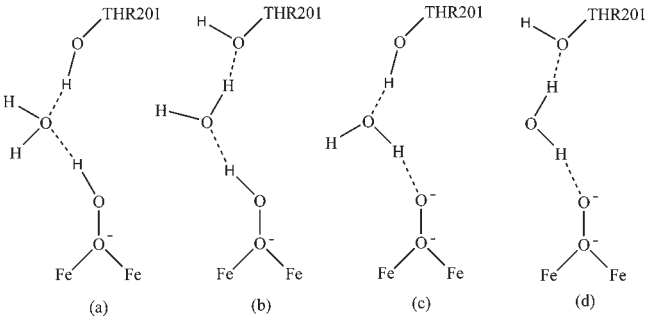

Figure 8. Possible hydrogen-bond networks stabilizing the peroxo structure of μ-1,1 coordination in the TMOHD complex. Models (a) and (b) are protonated.

noticeable difference in the isomer shift, it is the change in the quadrupole splitting parameter that is the most striking. The transition from ΔE = 1.51 mm/s in MMOH to ΔE = 0.67 mm/s in ToMOH may mean a significant alteration in the structure of the active site, most probably involving charged atoms or altered electron effects of the bound ligands, because such effects typically have a marked influence on the quadrupole splitting.[44−46]

As we noted before and as Table 4 reports, the computed Mössbauer characteristics of the peroxo structures shown in Figure 5 are totally incompatible with the experimental values. There may be several explanations for this discrepancy. Peroxo structures (a) and (b) in Figure 5 may be artifacts of TMOH because the TMOHD active site, involving an additional water molecule, might be essential for a proper modeling of peroxo intermediates and, consequently, reproduction of their Mössbauer spectra. However, this explanation appears improbable, because the substitution of the $O_2^{2-}\cdots$HO−Thr hydrogen bond by the $O_2^{2-}\cdots H_2O\cdots$HO−Thr hydrogen bond as a result of the complexation with the regulatory protein should not cause a significant change in the quadrupole splitting. Another, more plausible, explanation is that we did not sufficiently explore the configurational space in the course of the QM/MM optimization. Although we started with eight different peroxo models that converged to four distinct coordinations, many other geometries corresponding to local energy minima might exist, which either lie far from the starting geometries or which simply have not been found by the optimization algorithm. This problem is a common one of theoretical optimizations that involve several essential degrees of freedom and where the targeted geometry is not known for certain from experiment. Finally, the peroxo structure may be protonated, which may result in a significant change of the quadrupole splitting. From some studies[47,48] it can be inferred that certain protonated oxo-bridged diferric structures have much lower quadrupole splittings than their unprotonated analogs. This observation has a direct relevance to our predicament of matching the low quadrupole splitting of a peroxo species.

dx.doi.org/10.1021/ja110287y |*J. Am. Chem. Soc.* 2011, 133, 7384–7397

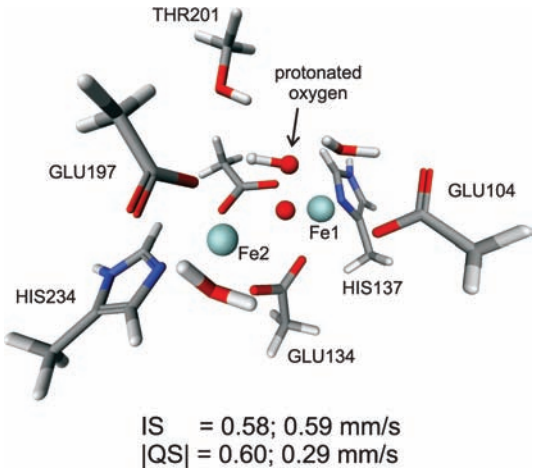

Figure 9. The geometry and the Mössbauer characteristics of one of the protonated model peroxo structures optimized with B3LYP (the μ-1,1 type coordination of the dioxygen molecule). The structure is shown in perspective in order to avoid atoms blotting one another; the only unlabeled residue is GLU231. The protonated distal oxygen atom is indicated. The color-coding is as follows: hydrogens are white, carbons are gray, oxygens are red, nitrogens are blue, and irons are cyan.

In order to address the two latter possibilities, we generated over 60 possible model peroxo diiron(III) structures within the ToMOH active site with the help of MC sampling. We presumed that sampling the T4moHD active site at this stage of the investigation would be undesirable because it would involve several extra degrees of freedom due to the additional water molecule, the presence of which would probably not contribute to significant changes in the quadrupole splitting parameters. Then, we computed the Mössbauer characteristics of all these structures, and none of the quadrupole splittings was close to the experimental value of ΔE = 0.67 mm/s for both iron atoms. We usually got quadrupole splittings having large values for both iron atoms, 1−3 mm/s, or one iron with a low value (less than 1 mm/s) while the other iron was characterized by a large value (over 2 mm/s), similar to the situation observed for peroxo structures (a) and (b) in Figure 5. It is only when we began to place protons on our model structures that we observed a significant drop in the quadrupole splittings of the resulting protonated species.

Figure 9 presents a DFT-optimized protonated model structure of the TMOH active site along with the corresponding Mössbauer characteristics, which are quite close to the experimental values. The isomer shift is 0.58 and 0.59 mm/s (two signals), and the quadrupole splitting is 0.60 and 0.29 mm/s. Even though this quadrupole splitting does not qualify as providing quantitative agreement with the experimental value (0.67 mm/s), it is qualitatively reasonable. The isomer shift is quite close (the corresponding experimental value is 0.54 mm/s), and both computed characteristics of the protonated structure are in sharp contrast with the computed Mössbauer characteristics of the unprotonated peroxo models from Figure 5 (see Table 4), which clearly contradict the experiment. We stress that the structure shown in Figure 9, with two bridging carboxylate groups and two water molecules, each coordinated to an iron atom, is only an approximate model obtained from a DFT minimization in the absence of the protein environment. We are not suggesting that it is necessarily representative of the true ToMOH peroxo structure.

We do not expect that a water molecule positioned in between the THR-201 residue and the hydroperoxo ion, in a manner sketched in Figure 8a and b, will have a significant effect on the quadrupole splitting because such a change involves uncharged entities that are relatively distant from the diiron core. We constructed a number of approximate protonated peroxo models in the manner of Figure 8a and b, starting from either the 3DHH crystal structure or the converged structures given in Figure 5. We also carried out constrained DFT optimizations of these models. This modeling yielded a cluster of at least 12 structures of varying similarity. Their Mössbauer spectra certainly differed, but one thing remained clear: the presence of an extra water hydrogen bonded with an OH group of T201, on one side, and the protonated peroxo group, on another, did not qualitatively deviate from the experimental Mössbauer spectrum of ToMOH peroxo intermediate. Most of our models had low values (<1.0 mm/s) of quadrupole splitting on both iron atoms, in accordance with our earlier observation for protonated peroxo models without the extra water molecule in the active site. For example, one manually built model protonated peroxo form with an extra water molecule in it gave the isomer shifts (IS) of 0.56 and 0.80 mm/s and the quadrupole splittings (QS) of 0.38 and 0.74 mm/s. Another similar model obtained as a result of a constrained DFT optimization gave IS of 0.63 and 0.70 mm/s and QS of 0.79 and 0.89 mm/s.

Our Mössbauer benchmarking work[35] tested Mössbauer spectra on a set of 31 diverse chemical structures and predicted mean unsigned errors of about 0.02 mm/s for the isomer shift and about 0.1 mm/s for the quadrupole splitting in the region <2.0 mm/s. The computed Mössbauer spectra of the TMOH peroxo models have significantly larger deviation from the reported experimental data. But the above error bounds were obtained on average-sized inorganic molecules with reliable crystal structures. When there is a great structural uncertainty and much more complicated chemical entities (proteins), as in the case of the ToMOH peroxo models, the errors are expected to increase. Therefore, given the approximate nature of our models, we consider our theoretical Mössbauer predictions to be in reasonable agreement with the experiment and the simpler protonated models illustrated by Figure 9.

A proper prediction of the ToMOH peroxo structure should involve a QM/MM modeling starting from the crystal structure with the regulatory protein attached. What the structure in Figure 9 illustrates is that, according to DFT, there exist stationary points of the protonated models which, at the same time, have Mössbauer characteristics that are quite close to the experimental ones. A meticulous study of similar protonated structures (also involving double protonation), both structural and spectroscopic, should be performed in the future following QM/MM optimization. Since the protonation is the only way we found to reconcile the low experimental quadrupole splitting with the theoretical predictions, the generation and the analysis of the protonated structures holds great promise for finding the right structure model for the ToMOH peroxo.

Recently, an X-ray structure of T4moH with H_2O_2 putatively bound to the active site was published (PDB 3I63).[15] Its examination reveals a H_2O_2 molecule loosely bound with the apparently ferric ions. The O−O distance (1.5 Å) in H_2O_2 is very similar to the distance in free H_2O_2, and the shortest distances between the iron atoms and the peroxide oxygen atoms (2.2 and 2.4 Å) are too long to indicate a true peroxo species. Additionally, our Mössbauer calculations based upon the model of this X-ray structure yield

the IS equal to 0.83 and 0.85 mm/s and the QS equal to 1.75 and 1.48 mm/s, which is in obvious disagreement with the experimental data (IS = 0.56 mm/s, QS = 0.67 mm/s). All these details make us regard this structure as T4moH cocrystallized with H_2O_2 rather than a protonated peroxo T4moH. As such, it probably has little relevance for the actual geometry of the peroxo species.

RELATION TO CYTOCHROME P450

Cytochrome P450 enzymes comprise a family of oxygenases structurally and physiologycally unrelated to BMM.[49] There is little common between the active sites of the two families because the former has a monoiron, thiolate-coordinated heme center and the latter are diiron enzymes that are rich in carboxylate ligands. However, there are striking similarities between the oxygen activation mechanisms of these two families.

The first similarity is the presence of adjacent threonine and asparagine side chains in the vicinity of the active sites of BMM and P450 enzymes. The P450 research community has established an important role that these two residues play in the delivery of protons needed for dioxygen activation.[50−53] Similar function was proposed for these two residues in BMM enzymes.[14,17,21,39,40] More evidence for a similar functional role of the threonine residue in BMM and P450 active sites comes from mutagenesis studies in TMOH and P450 enzymes. Substituting the threonine with residues incapable of forming hydrogen bond with the dioxygen in the active site severely disrupts hydroxylation in either ToMOH,[17] T4moH,[40] or P450.[23,54,55] In contrast, replacing the threonine with serine, thus preserving a hydrogen-bond forming hydroxyl group, alters oxidation mechanism but preserves the oxidative capabilities of either ToMOH[14] or P450.[54]

Another analogy between P450 and BMM families concerns the nature of the peroxo intermediate. There seems to be a consensus regarding the molecular geometry of the so-called Compound 0, a distally protonated peroxo intermediate of P450 enzymes.[56−58] The present work also suggests a distally protonated structure for the TMOH peroxo intermediate based on QM/MM and Mössbauer spectra modeling, providing another link with the P450 oxidative mechanism.

It is unlikely, however, that the parallels between the oxidative mechanisms of BMM and P450 families continue beyond the hydroxyperoxo species. In P450, the oxidation is primarily performed by Compound I, an Fe(IV) radical cation. In MMOH the principal oxidant is an Fe(IV)−Fe(IV) species Q,[10,42,43] whereas in TMOH no oxidative species other than peroxo has been observed.[13] Nevertheless, the similarity between the proton-shuttling hydrogen-bonding network formed with identical residues near the active site as well as an analogous protonation of the peroxo intermediate during the dioxygen activation in two unrelated active sites suggests an intriguing example of convergent mechanistic evolution.

CONCLUSION

Nature surpasses human imagination in how it can utilize small modifications in biomolecules in order to fine-tune biochemical processes or produce drastic changes in the phenotype. Countless examples are known where the difference of one hydrogen bond or a single amino acid causes macro-effects. Bacteria with a metabolism that depends upon BMMs seem to exploit small variations in these protein structures for better adaptation to their biological niche. In this work we have examined the structural differences between the two classes of BMM enzymes, MMOH and TMOH, the active sites of which are almost identical, and yet their chemistry is markedly divergent. We focus on the process of dioxygen activation, which produces different types of peroxo species in MMOH and TMOH, according to spectroscopic measurements.

After listing and discussing some notable amino acid differences in the vicinity of the MMOH and TMOH active sites, we cannot find a clear explanation as to how any of these changes can bring about the disparate chemistry of the dioxygen activation of the two enzymes. Then, we narrowed our analysis to the strictly conserved threonine residue in the BMM family (T213 in MMOH and T201 in TMOH) and demonstrated that, in all the nonperturbed crystal structures of MMOH, T213 has a rotational configuration along its $C_\alpha-C_\beta$ bond that is qualitatively distinct from the configuration of T201 in all the crystal structures of TMOH. A series of rotational profiles around the $C_\alpha-C_\beta$ bond of the threonine side chain that we generated using both MM and QM/MM methods are in good agreement with experimental observations and helps explain the formation of two peroxo species in the case of the T201S mutant. According to the rotational energy profiles, the regulatory protein imposes a very tall barrier on rotation of the threonine side chain, perhaps controlling specificity in the formation of the peroxo species of the wild-type proteins. A more detailed study involving other mutants, both theoretically and experimentally, is reserved for the future, to either confirm or refute the hypothesis that the configuration of the threonine is directly related to the formation of one or another type of peroxo species.

Our QM/MM geometry optimizations of the peroxo and Q intermediates of TMOH starting from the 2INC crystal structure (not involving the regulatory protein) demonstrate that the most stable peroxo form, of the μ-1,2 type coordination of the oxygen and stabilized by the hydrogen bond that the peroxo-anion forms with the threonine hydroxyl, is nearly 5 kcal/mol more stable than the Q structure. This result is in contrast to our recent investigation of the MMOH intermediates[10] in which it was shown that the peroxo and Q structures have an almost equal energy. The present computational result is in agreement with experiment, which does not detect a Q form for ToMOH. The computed Mössbauer parameters of the optimized peroxo structures are in disagreement with experiment, and we propose a number of explanations for this fact. In particular, we show that protonation of the peroxo unit can reconcile theoretical and experimental Mössbauer data. Finally, we argue that it will be important to undertake a QM/MM study based on the T4moHD crystal structure, since this structure should be relevant to the intermediates observed in experiment.

More work is required to clarify several remaining issues: the structure of the $ToMOH_{peroxo}$ intermediate and its possible protonation and stabilization through the hydrogen-bonding network involving T201, the relative stability of the peroxo with respect to the Q structure, and the further analysis of the hypothesis (through the studies of the mutant forms) that T201 in TMOH and T213 in MMOH plays a key role in the formation of the peroxo species. However, we believe that the present study, through the insights into the function of the threonine residue, the role of the regulatory protein, and the possibility of protonation at a suitable location in the active site to explain the $ToMOH_{peroxo}$ quadrupole splitting, paves the way toward future progress in understanding the chemistry of the TMOH and MMOH intermediates.

Finally, we wish to highlight the elevated objectives set for the computational methodology in this work. Applying high-level computational tools, such as QM/MM, to single protein systems as well as comparing multiple proteins by bioinformatics-type treatments has become relatively straightforward. But using high-level computations for understanding differences in chemical behavior of large, highly homologous proteins is still a great challenge. This work demonstrates a successful approach to this kind of problem and helps define the aims for the future progress in this area.

■ ASSOCIATED CONTENT

Supporting Information. The Supporting Information contains the complete citation of ref 25 and the atomic coordinates of the structures displayed in Figures 5 and 9. This material is available free of charge via the Internet at http://pubs.acs.org/.

■ AUTHOR INFORMATION

Corresponding Author
rich@chem.columbia.edu; lippard@mit.edu

■ ACKNOWLEDGMENT

R.A.F. acknowledges grant no. GM40526 from the National Institute of Health, and S.J.L. acknowledges grant no. GM032134 from the National Institute of General Medical Sciences.

■ REFERENCES

(1) Leahy, J. G.; Batchelor, P. J.; Morcomb, S. M. *FEMS Microbiol. Rev.* **2003**, *27*, 449–479.
(2) Notomista, E.; Lahm, A.; Di Donato, A.; Tramontano, A. *J. Mol. Evol.* **2003**, *56*, 435–445.
(3) Sazinsky, M. H.; Lippard, S. J. *Acc. Chem. Res.* **2006**, *39*, 558–566.
(4) Murray, L. J.; Lippard, S. J. *Acc. Chem. Res.* **2007**, *40*, 466–474.
(5) Wallar, B. J.; Lipscomb, J. D. *Chem. Rev.* **1996**, *96*, 2625–2658.
(6) Merkx, M.; Kopp, D. A.; Sazinsky, M. H.; Blazyk, J. L.; Müller, J.; Lippard, S. J. *Angew. Chem., Int. Ed.* **2001**, *40*, 2782–2807.
(7) Kopp, D. A.; Lippard, S. J. *Curr. Opin. Chem. Biol.* **2002**, *6*, 568–576.
(8) Baik, M.-H.; Newcomb, M.; Friesner, R. A.; Lippard, S. J. *Chem. Rev.* **2003**, *103*, 2385–2420.
(9) Gherman, B. F.; Baik, M.-H.; Lippard, S. J.; Friesner, R. A. *J. Am. Chem. Soc.* **2004**, *126*, 2978–2990.
(10) Rinaldo, D.; Philipp, D. M.; Lippard, S. J.; Friesner, R. A. *J. Am. Chem. Soc.* **2007**, *129*, 3135–3147.
(11) Han, W.-G.; Noodleman, L. *Inorg. Chem. Acta* **2008**, *361*, 973–986.
(12) Tinberg, C. E.; Lippard, S. J. *Biochemistry* **2009**, *48*, 12145–12158.
(13) Murray, L. J.; Naik, S. G.; Ortillo, D. O.; García-Serres, R.; Lee, J. K.; Huynh, B. H.; Lippard, S. J. *J. Am. Chem. Soc.* **2007**, *129*, 14500–14510.
(14) Song, W. J.; Behan, R. K.; Naik, S. G.; Huynh, B. H.; Lippard, S. J. *J. Am. Chem. Soc.* **2009**, *131*, 6074–6075.
(15) Bailey, L. J.; Fox, B. G. *Biochemistry* **2009**, *48*, 8932–8939.
(16) Notomista, E.; Cafaro, V.; Bozza, G.; Di Donato, A. *Appl. Environ. Microbiol.* **2009**, *75*, 823–836.
(17) Song, W. J.; McCormick, M. S.; Behan, R. K.; Sazinsky, M. H.; Jiang, W.; Lin, J.; Krebs, C.; Lippard, S. J. *J. Am. Chem. Soc.* **2010**, *132*, 13582–13585.
(18) Sazinsky, M. H.; Bard, J.; Di Donato, A.; Lippard, S. J. *J. Biol. Chem.* **2004**, *279*, 30600–30610.
(19) McCormick, M. S.; Sazinsky, M. H.; Condon, K. L.; Lippard, S. J. *J. Am. Chem. Soc.* **2006**, *128*, 15108–15110.
(20) Murray, L. J.; García-Serres, R.; McCormick, M. S.; Davydov, R.; Naik, S. G.; Kim, S.-H.; Hoffman, B. M.; Huynh, B. H.; Lippard, S. J. *Biochemistry* **2007**, *46*, 14795–14809.
(21) Bailey, L. J.; McCoy, J. G.; Phillips, G. N., Jr.; Fox, B. G. *Proc. Natl. Acad. Sci. U.S.A.* **2008**, *105*, 19194–19198.
(22) Raag, R.; Martinis, S. A.; Sligar, S. G.; Poulos, T. L. *Biochemistry* **1991**, *30*, 11420–11429.
(23) Altarsha, M.; Benighaus, T.; Kumar, D.; Thiel, W. *J. Am. Chem. Soc.* **2009**, *131*, 4755–4763.
(24) Li, X.; Jacobson, M. P.; Zhu, K.; Zhao, S.; Friesner, R. A. *Proteins: Struct., Funct., Bioinf.* **2007**, *66*, 824–837.
(25) Banks, J. L.; et al. *J. Comput. Chem.* **2005**, *26*, 1752–1780.
(26) *QSite 4.5*; Schrödinger, Inc.: Portland, OR, 2007.
(27) Murphy, R. B.; Philipp, D. M.; Friesner, R. A. *Chem. Phys. Lett.* **2000**, *321*, 113–120.
(28) Murphy, R. B.; Philipp, D. M.; Friesner, R. A. *J. Comput. Chem.* **2000**, *21*, 1442–1457.
(29) Philipp, D. M.; Friesner, R. A. *J. Comput. Chem.* **1999**, *20*, 1468–1494.
(30) Hay, P. J.; Wadt, W. R. *J. Chem. Phys.* **1985**, *82*, 270–283.
(31) Hay, P. J.; Wadt, W. R. *J. Chem. Phys.* **1985**, *82*, 299–310.
(32) Wadt, W. R.; Hay, P. J. *J. Chem. Phys.* **1985**, *82*, 284–298.
(33) Kolossváry, I.; Guida, W. C. *J. Comput. Chem.* **1999**, *20*, 1671–1684.
(34) Keserû, G.; Kolossváry, I. *J. Am. Chem. Soc.* **2001**, *123*, 12708–12709.
(35) Bochevarov, A. D.; Friesner, R. A.; Lippard, S. J. *J. Chem. Theory Comput.* **2010**, *6*, 3735–3749.
(36) Elango, N. A.; Radhakrishnan, R.; Froland, W. A.; Wallar, B. J.; Earhart, C. A.; Lipscomb, J. D.; Ohlendorf, D. H. *Protein Sci.* **1997**, *6*, 556–568.
(37) Coufal, D. E.; Blazyk, J. L.; Whittington, D. A.; Wu, W. W.; Rosenzweig, A. C.; Lippard, S. J. *Eur. J. Biochem.* **2000**, *267*, 2174–2185.
(38) Pikus, J. D.; Mitchell, K. H.; Studts, J. M.; McClay, K.; Steffan, R. J.; Fox, B. G. *Biochemistry* **2000**, *39*, 791–799.
(39) Sazinsky, M. H.; Dunten, P. W.; McCormick, M. S.; Di Donato, A.; Lippard, S. J. *Biochemistry* **2006**, *45*, 15392–15404.
(40) Elsen, N. L.; Bailey, L. J.; Hauser, A. D.; Fox, B. G. *Biochemistry* **2009**, *48*, 3838–3846.
(41) Han, W.-G.; Noodleman, L. *Inorg. Chem.* **2008**, *47*, 2975–2986.
(42) Brunold, T. C.; Tamura, N.; Kitajima, N.; Moro-oka, Y.; Solomon, E. I. *J. Am. Chem. Soc.* **1998**, *120*, 5674–5690.
(43) Yumura, T.; Yoshizawa, K. *Bull. Chem. Soc. Jpn.* **2004**, *77*, 1305–1311.
(44) Ohya, T.; Sato, M. *J. Chem. Soc., Dalton Trans.* **1996**, *8*, 1519–1523.
(45) Cao, C.; Dahal, S.; Shang, M.; Beatty, A. M.; Hibbs, W.; Schulz, C. E.; Scheidt, W. R. *Inorg. Chem.* **2003**, *42*, 5202–5210.
(46) Guerriero, P.; Tamburini, S; Vigato, P. A.; Russo, U.; Benelli, C. *Inorg. Chim. Acta* **1993**, *213*, 279–287.
(47) Wu, F.-J.; Kurtz, D. M., Jr.; Hagen, K. S.; Nyman, P. D.; Debrunner, P. G.; Vankai, V. A. *Inorg. Chem.* **1990**, *29*, 5174–5183.
(48) Tshuva, E. Y.; Lippard, S. J. *Chem. Rev.* **2004**, *104*, 987–1012.
(49) Ortiz de Montellano, P. R. *Cytochrome P450: Structure, Mechanism and Biochemistry*, 3rd ed.; Plenum Press: New York, 2005.
(50) Gerber, N. C.; Sligar, S. G. *J. Biol. Chem.* **1994**, *269*, 4260–4266.
(51) Vidakovic, M.; Sligar, S. G.; Li, H.; Poulos, T. L. *Biochemistry* **1998**, *37*, 9211–9219.
(52) Clark, J. P.; Miles, C. S.; Mowat, C. G.; Walkinshaw, M. D.; Reid, G. A.; Daff, S. N.; Chapman, S. K. *J. Inorg. Biochem.* **2006**, *100*, 1075–1090.
(53) Hlavica, P. *Eur. J. Biochem.* **2004**, *271*, 4335–4360.
(54) Imai, M.; Shimada, H.; Matsushima-Hibaya, Y.; Makino, R.; Koga, H.; Horiuchi, T.; Ishimura, Y. *Proc. Natl. Acad. Sci. U.S.A.* **1989**, *86*, 7823–7827.
(55) Yeom, H.; Sligar, S. G.; Li, H.; Poulos, T. L.; Fulco, A. J. *Biochemistry* **1995**, *34*, 14733–14740.

(56) Davydov, R.; Makris, T. M.; Kofman, V.; Werst, D. E.; Sligar, S. G.; Hoffman, B, M. *J. Am. Chem. Soc.* **2001**, *123*, 1403–1415.
(57) Groenhof, A.; Ehlers, A. W.; Lammertsma, K. *J. Am. Chem. Soc.* **2007**, *129*, 6204–6209.
(58) Altun, A.; Kumar, D.; Neese, F.; Thiel, W. *J. Phys. Chem. A* **2008**, *112*, 12904–12910.